5. KOHONEN'S NETWORK FOR MODELING THE AUDITORY CORTEX OF A BAT

In this chapter we employ Kohonen's model to simulate the projection of the space of the ultrasound frequencies onto the auditory cortex of a bat (Martinetz, Ritter, and Schulten 1988). The auditory cortex is the area of the cerebrum responsible for sound analysis (Kandel and Schwartz, 1985). We will compare the results of the simulation with available measurements from the cortex of the bat *Pteronotus parnelli rubiginosus*, as well as with an analytic calculation.

For each animal species, the size of an area of neural units responsible for the analysis of a particular sense strongly depends on the importance of that sense for the species. Within each of those areas the extent of the cortical representation of each input stimulus depends on the required resolution. For example, the fine analysis of the visual information of higher mammals is accomplished in the *fovea*. The fovea is a very small area of the retina in the vicinity of the optical axis with a very high density of *rods* and *cones*, the light sensitive receptors in the eye. The especially high density gives rise to a significantly higher resolution in this area than in the regions of the retina responsible for the peripheral part of the visual field. Although the fovea is only a small part of the total retina, the larger part of the visual cortex is dedicated to the processing of signals from the fovea. Similarly nonproportional representations have also been found in the somatosensory system and in the motor cortex. For example, particularly large areas in the somatosensory and the motor cortex are assigned to the hand when compared to the area devoted to the representation of other body surfaces or limbs (Woolsey 1958).

In contrast no nonproportional projections have been found so far in the auditory cortex of higher mammals. The reason for this is perhaps that the acoustic signals perceived by most mammals contain a wide spectrum of frequencies; the signal energy is usually not concentrated in a narrow range of frequencies. The meow of a cat, for example, is made up of many

harmonics of the base tone, and no region of the frequency spectrum plays any particular function in the cat's survival. The auditory cortex of cats was thoroughly examined, and the result was that frequencies, as expected, are mapped onto the cortex in a linearly increasing arrangement without any regard for particular frequencies. The high-frequency units lie in the *anterior* and the low-frequency units lie in the *posterior* region of the cortex. According to available experimental evidence, the auditory cortex of dogs and monkeys is structured very similarly (Merzenich et al. 1975).

5.1   The Auditory Cortex of a Bat

In bats, nonproportional projections have been detected in the auditory cortex. Due to the use of sonar by these animals, the acoustic frequency spectrum contains certain intervals which are more important. Bats utilize a whole range of frequencies for orientation purposes. They can measure the distances to objects in their surroundings by the time delay of the echo of their sonar signals, and they obtain information about the size of the detected objects by the amplitude of the echo.

In addition, bats are able to determine their flight velocity relative to other objects by the Doppler shift of the sonar signal that they transmit. This ability to determine the Doppler shift has been intensively studied in *Pteronotus parnelli rubiginosus*, a bat species which is native to Panama (Suga and Jen 1976). This species has developed this ability to the extent that it is able to resolve relative velocities up to 3 cm/s, enabling it to detect even the beating of the wings of insects, its major source of nutrition. The transmitted sonar signal consists of a pulse that lasts about 30 ms at a frequency of 61 kHz. For the analysis of the Doppler-shifted echoes, this bat employs a special part of its auditory cortex (Suga and Jen 1976).

The Doppler shift Δf of the sonar frequency by an object moving in the same line with the bat is determined by

$$\frac{\Delta f}{f_e} = \frac{2v_{bat}}{c} - \frac{2v_{obj}}{c}. \tag{5.1}$$

Here f_e is the bat's sonar frequency, *i.e.*, 61 kHz, v_{bat} is the bat's velocity, v_{obj} is the object's flight velocity, and c is the velocity of sound. The factor of two is due to the fact that both the transmitted signal and the echo are Doppler shifted. If the bat knows its own velocity, it can determine v_{obj} from the Doppler shift Δf.

Excellent sonar capabilities are certainly indispensable for the bat's survival. To be able to detect a frequency shift of 0.02% which corresponds to the stated relative velocity of 3 cm/s, assuming a sound velocity of 300 m/s, a particularly high resolution of frequencies around the sonar frequency is necessary. Therefore, it would not be surprising if the interval around 61 kHz of the frequency spectrum were disproportionately represented in the part of the auditory cortex responsible for the Doppler analysis. Investigations on *Pteronotus parnelli rubiginosus* indeed support this expectation (Suga and Jen 1976).

Figure 5.1 shows the results of observations by Suga and Jen (1976). In part B of Fig. 5.1 one can clearly see that the one-dimensional frequency spectrum essentially extends continuously and monotonically from the posterior to the anterior region of the auditory cortex. In addition, one recognizes a region around the sonar frequency of 61 kHz with a very high resolution. To emphasize this anomaly, the region shaded in part A of Fig 5.1 has been displayed separately in part C. This region corresponds to the frequency interval which is especially important for the bat and extends monotonically from a minimum frequency of about 20 kHz up to a maximum frequency of about 100 kHz. The position and *best frequency* for each measurement in the shaded region of A is also shown in part C of Fig. 5.1. As "best frequency" for a neuron, one picks the frequency that causes the highest excitation of that neuron. One clearly sees that the majority of the measured values are clustered around the sonar frequency, as is expected. Almost half of the anterior-posterior region is used for the analysis of the Doppler-shifted signals. This provides the particularly high resolution of 0.02% which gives the bat its fine navigational and insect hunting abilities.
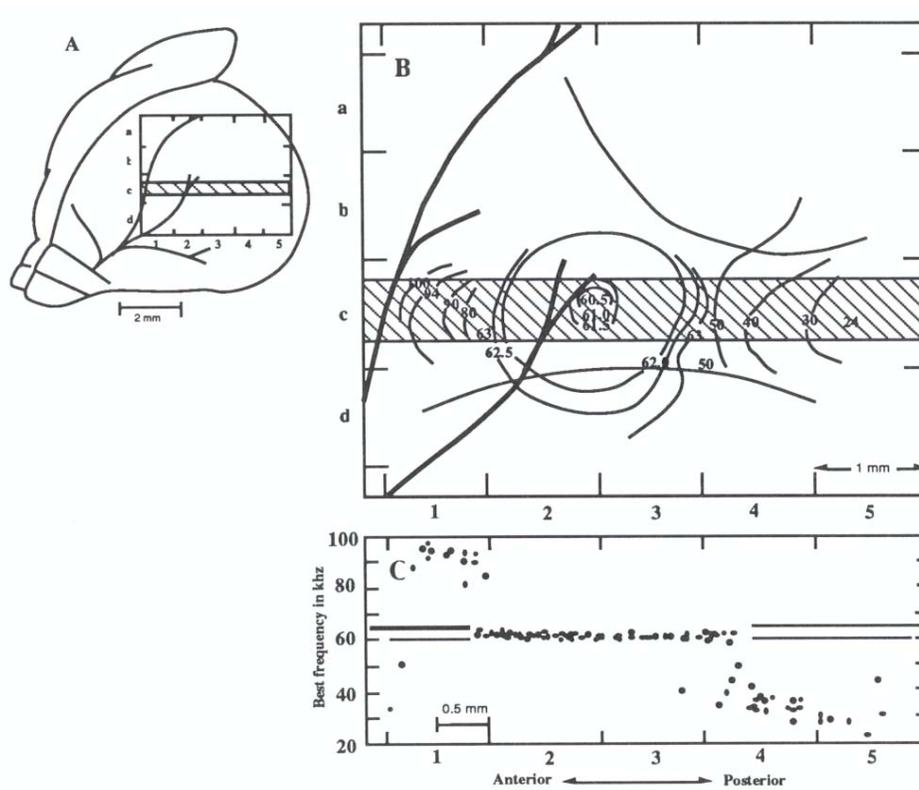
Abb. 5.1: (A) Dorsolateral view of the bat's cerebrum. The auditory cortex lies within the inserted rectangle. (B) Distribution of "best frequencies" on the auditory cortex, the rectangle in (A). (C) Distribution of "best frequencies" along the region shaded in (A) and (B). The distribution of measured values around 61 kHz has been enlarged (after Suga and Jen 1976).

5.2 A Model of the Bat's Auditory Cortex

The development of the projection of the one-dimensional frequency space onto the auditory cortex, with special weighting of the frequencies around 61 kHz, will now be simulated by Kohonen's model of self-organizing maps. For this purpose we will model the auditory cortex by an array of 5×25 neural units.

The space of input stimuli is the one-dimensional ultrasound spectrum of the

bat's hearing. In our model this spectrum will be simulated by a Gaussian distribution of Doppler-shifted sonar echoes on top of a white background noise. The background noise in the range from 20 to 100 kHz depicts signals from external ultrasound sources. In addition, there is a peak near 61 kHz which consists of the echoes from objects moving relative to the bat. We describe this peak of Doppler-shifted sonar signals by a Gaussian distribution centered at 61 kHz with a width of σ_r=0.5 kHz. This corresponds to a root mean square speed difference of the sonar-detected objects of about 2 m/s. Doppler-shifted sonar signals occur in our model three times as often as signals from the white background noise. Figure 5.2 shows the weighted probability distribution.
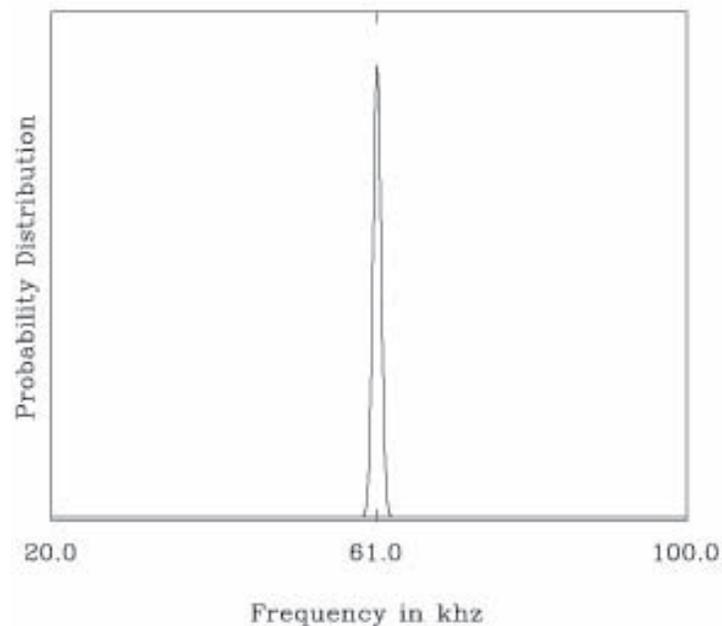
Abb. 5.2: The relative probability density of the input signals versus frequency. Doppler-shifted echoes occur exactly three times as often as signals from the white background noise.

Initially, a random frequency is assigned to each model neuron of our model cortex. This corresponds to Step 0 of Kohonen's model as described in the last chapter. Due to the one-dimensionality of the space of input stimuli, the

synaptic strengths $\mathbf{w_r}$ of the model neurons $\mathbf{r}$ have only a single component.[1]
An input signal according to a probability distribution $P(\mathbf{v})$ causes that
model neuron whose momentarily assigned frequency (the so-called "best
frequency" of that neuron) lies closest to the input frequency to determine the
center of the "activity peak" within which the neurons become significantly
excited (Step 2). Next, the "best frequencies" of all neurons of the cortex
are modified according to Step 3 of Kohonen's algorithm. After a sufficient
number of steps this modification should result in an arrangement of "best
frequencies" on the model cortex that is continuous and is adapted to the
particular probability distribution of the input signals.

5.3   Simulation Results

In Fig. 5.1B it can be seen that the region of the auditory cortex of *Pterono-
tus parnelli rubiginosus* responsible for the resolution of the echo is greatly
elongated, it being much more extended along the anterior-posterior axis
than it is along the perpendicular direction. A similar length-width ratio for
the model cortex was chosen in the simulation we will describe. There, the
anterior-posterior length contains 25 model neurons and is five times longer
than the width of the array.
Figure 5.3 shows the model cortex at different stages of the learning process.
Each model neuron is represented by a box containing (the integer part of)
the assigned frequency. Figure 5.3a presents the initial state. Each neuron
was assigned randomly a frequency value in the range 20 to 100 kHz. As
we see in Fig. 5.3.b, after 500 learning steps a continuous mapping between
the space of input frequencies and the model cortex has already emerged.
The final state, achieved after 5000 learning steps, is depicted in Fig. 5.3.c.
One can see the special feature of Kohonen's model that represents the input
stimuli on the net of neural units according to the probability with which
stimuli occur. The strong maximum of the probability density in our model
causes a wide-ranging occupation of the "cortex" with frequencies in the
narrow interval around the sonar frequency of 61 kHz.

---

[1] This is only an idealization that is caused by the explicit use of frequency values. In
a more realistic model one could, for example, code the frequency by different output
amplitudes of a set of overlapping filters as they are actually realized in the inner ear.
The ordering process demonstrated in the simulation would, however, not be affected
by this.

78	45	63	43	75
51	77	28	86	91
52	80	24	34	45
52	85	91	85	84
23	97	26	27	37
96	28	98	86	82
44	99	50	81	42
52	86	74	92	75
66	39	56	41	34
99	23	77	69	61
42	47	81	38	100
93	86	56	45	23
36	70	46	59	22
62	59	80	97	25
64	92	94	23	84
83	59	31	89	47
76	71	41	41	89
72	27	85	27	67
51	23	93	100	27
89	52	32	42	65
48	44	30	65	45
21	34	83	77	31
25	38	82	38	79
47	75	43	86	64
20	73	43	51	64

28	28	30	32	35
28	29	31	33	36
30	31	32	35	37
33	33	35	37	39
36	37	38	39	41
40	41	41	43	44
44	44	45	46	47
48	48	49	49	50
51	52	52	52	53
54	54	55	55	55
57	57	57	57	57
58	58	58	58	58
59	59	59	59	59
60	60	60	60	60
60	60	60	60	60
60	60	60	60	60
60	60	60	60	60
60	60	60	60	60
61	61	61	61	61
62	61	61	61	61
62	62	62	62	62
63	63	63	63	62
64	64	63	63	63
64	64	64	64	63
65	64	64	64	64

36	33	29	26	25
38	35	32	30	27
40	39	37	35	33
44	42	41	39	39
47	46	44	44	44
50	49	48	48	49
54	53	53	54	54
58	58	58	58	58
59	59	59	59	59
60	60	60	60	60
60	60	60	60	60
61	61	61	61	61
61	61	61	61	61
61	61	61	61	61
61	61	61	61	61
62	62	62	62	62
62	62	62	62	63
62	62	63	63	63
64	64	64	64	65
68	68	68	69	68
72	73	73	74	73
75	77	79	81	81
78	80	84	87	88
81	83	87	91	93
82	85	90	94	98

Abb. 5.3: (a) (left) The initial state with random frequencies assigned to the neural units. The length-to-width ratio of the array of model neurons is five (anterior-posterior) to one (dorsolateral). Each box represents a neuron and contains the integer part of the current "best frequency" assigned to that neuron. (b) (middle) The state of the "auditory cortex" after 500 learning steps. The field has evolved into a state where neighboring neurons have similar "best frequencies;" i.e., the space of input stimuli is represented continuously on the array. (c) (right) The "auditory cortex" in the final state, after 5000 learning steps. The region of "best frequencies" around the sonar frequency, which represents the Doppler-shifted input signals, occupies almost half of the model cortex.

In this simulation the time dependence of the excitation zone σ and of the adaptation step widths ϵ were chosen as follows: $\sigma(t) = \sigma_i[1+\exp(-5\,(t/t_{max})^2)]$ and $\epsilon(t) = \epsilon_i \exp(-5\,(t/t_{max})^2)$ with $\sigma_i = 5$ and $\epsilon_i = 1$, where t denotes the number of performed learning steps. The final number of learning steps at the end of the simulation was $t_{max} = 5000$.

Abb. 5.4: The simulation results presented as in Fig. 5.1C. Along the abscissa are the positions 1 through 25 of the model neurons along the "anterior-posterior" axis. The ordinate shows the corresponding "best frequencies." For every value between 1 and 25 five frequency values are represented, one for each of the five neural units along the "dorso-lateral" direction.

In accordance with the experimental results from the auditory cortex of *Pteronotus parnelli rubiginosus*, the representation of the input frequencies on our model cortex increases monotonically along the "anterior-posterior" axis. In order to compare the results of our simulation with the measurements, we have presented the distribution of "best frequencies" as in Fig. 5.1C. Figure 5.4 depicts the simulation results of Fig. 5.3 in the same way as Fig. 5.1C represents the data of Fig. 5.1A-B. Each model neuron has been described by its position 1 to 25 on the "anterior-posterior" axis as well as by its "best frequency." This representation of the results of the simulation produces a picture very similar to that of the experimental measurements (Fig. 5.1). In both cases a plateau arises that occupies almost half of the cortex and contains the neural units specialized in the analysis of the Doppler-shifted echoes. The size of this plateau is determined by the shape of the probability distribution of the input stimuli. In Section 5.4 we will look more closely at the relation between the shape of the probability distribution and the final cortical representation in Kohonen's model.

5.4 Mathematical Description of the "Cortical Representation"

We want to investigate what mappings between a neural lattice and an input signal space result asymptotically for Kohonen's model. For "maximally ordered" states we will demonstrate a quantitative relation between the "neural-occupation density" in the space of input stimuli which corresponds to the local enlargement factor of the map, and the functional form of the probability density $P(\mathbf{v})$ of the input signals (Ritter and Schulten 1986a). The result will enable us to derive an analytical expression for the shape of the curve shown in Fig. 5.4, including the size of the plateau. Unfortunately, such analytical expressions will be limited to the special case of one-dimensional networks and one-dimensional input spaces. The following derivation is mainly directed at the mathematically inclined reader; it can be skipped without loss of continuity.

To begin, we consider a lattice A of N formal neurons $\mathbf{r}_1, \mathbf{r}_2,$ $\ldots, \mathbf{r}_N$. A map $\phi_{\mathbf{w}} : V \mapsto A$ of the space V onto A, which assigns to each element $\mathbf{v} \in V$ an element $\phi_{\mathbf{w}}(\mathbf{v}) \in A$, is defined by the synaptic strengths $\mathbf{w} = (\mathbf{w}_{\mathbf{r}_1}, \mathbf{w}_{\mathbf{r}_2}, \ldots, \mathbf{w}_{\mathbf{r}_N})$, $\mathbf{w}_{\mathbf{r}_j} \in V$. The image $\phi_{\mathbf{w}}(\mathbf{v}) \in A$ that belongs to $\mathbf{v} \in V$ is specified by the condition

$$\|\mathbf{w}_{\phi_{\mathbf{w}}(\mathbf{v})} - \mathbf{v}\| = \min_{\mathbf{r} \in A} \|\mathbf{w}_{\mathbf{r}} - \mathbf{v}\|, \tag{5.2}$$

i.e., an element $\mathbf{v} \in V$ is mapped onto that neuron $\mathbf{r} \in A$ for which $\|\mathbf{w}_{\mathbf{r}} - \mathbf{v}\|$ becomes minimal.

As described in Chapter 4, $\phi_{\mathbf{w}}$ emerges in a learning process that consists of iterated changes of the synaptic strengths $\mathbf{w} = (\mathbf{w}_{\mathbf{r}_1}, \mathbf{w}_{\mathbf{r}_2}, \ldots, \mathbf{w}_{\mathbf{r}_N})$. A learning step that causes a change from $\mathbf{w}'$ to $\mathbf{w}$ can formally be described by the transformation

$$\mathbf{w} = \mathbf{T}(\mathbf{w}', \mathbf{v}, \epsilon). \tag{5.3}$$

Here $\mathbf{v} \in V$ represents the input vector invoked at a particular instance, and ϵ is a measure of the plasticity of the synaptic strengths (see Eq. (4.15).

The learning process is driven by a sequence of randomly and independently chosen vectors $\mathbf{v}$ whose distribution obeys a probability density $P(\mathbf{v})$. The transformation (5.3) then defines a Markov process in the space of synaptic strengths $\mathbf{w} \in V \otimes V \otimes \ldots \otimes V$ that describes the evolution of the map $\phi_{\mathbf{w}}(\mathbf{v})$. We will now show that the stationary state of the map which evolves asymp-

totically by this process can be described by a partial differential equation for the stationary distribution of the synaptic strengths.

Since the elements $\mathbf{v}$ occur with the probability $P(\mathbf{v})$, the probability $Q(\mathbf{w}, \mathbf{w}')$ for the transition of a state $\mathbf{w}'$ to a state $\mathbf{w}$, via adaptation step (5.3), is given by

$$Q(\mathbf{w}, \mathbf{w}') = \int \delta(\mathbf{w} - \mathbf{T}(\mathbf{w}', \mathbf{v}, \epsilon)) P(\mathbf{v}) \, d\mathbf{v}. \tag{5.4}$$

$\delta(\mathbf{x})$ denotes the so-called delta-function which is zero for all $\mathbf{x} \neq 0$ and for which $\int \delta(\mathbf{x}) d\mathbf{x} = 1$. More explicitly, Eq. (5.3) can be written

$$\mathbf{w}_\mathbf{r} = \mathbf{w}'_\mathbf{r} + \epsilon \, h_\mathbf{rs}(\mathbf{v} - \mathbf{w}'_\mathbf{r}) \quad \text{for all } \mathbf{r} \in A. \tag{5.5}$$

Here $\mathbf{s} = \phi_{\mathbf{w}'}(\mathbf{v})$ is the formal neuron to which $\mathbf{v}$ is assigned in the old map $\phi_{\mathbf{w}'}$.

In the following we take exclusive interest in those states $\phi_\mathbf{w}$ that correspond to "maximally ordered maps," and we want to investigate their dependence on the probability density $P(\mathbf{v})$. We assume that the space V and the lattice A have the same dimensionality d. A "maximally ordered map" can then be characterized by the condition that lines in V which connect the $\mathbf{w}_\mathbf{r}$ of $\mathbf{r}$ adjacent in the network are not allowed to cross. Figure 5.5 demonstrates this fact with an example of a two-dimensional Kohonen lattice on a two-dimensional space V of input stimuli with a homogeneous probability distribution $P(\mathbf{v})$. The square frame represents the space V. The synaptic strengths $\mathbf{w}_\mathbf{r} \in V$ determine the locations on the square which are assigned to the formal neurons $\mathbf{r} \in A$. Each mesh point of the lattice A corresponds to a formal neuron and, in our representation, is drawn at the location that has been assigned to that neuron through $\mathbf{w}_\mathbf{r}$. Two locations $\mathbf{w}_\mathbf{r}$ are connected by a line if the two corresponding formal neurons $\mathbf{r}$ are neighbors in the lattice A. Figure 5.5a shows a map that has reached a state of "maximal order" as seen by the lack of line crossings between lattice points. In contrast Fig. 5.5b presents a map for which even in the final stage some connections still cross. Such a map is not "maximally ordered."

In the following calculation we will make a transition from discrete values of $\mathbf{r}$ to continuous ones. This is possible because in the following we restrict ourselves to "maximally ordered" states where in the transition to a continuum $\mathbf{w}_\mathbf{r}$ becomes a smooth function of the spatial coordinate $\mathbf{r}$ in the network.
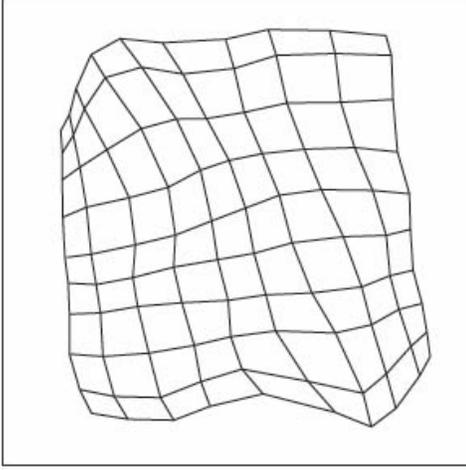
Abb. 5.5: An example for a "maximally ordered" state of the network. Network and input signals are both two-dimensional. All input signals originate from the limiting square. In the continuum limit the network nodes are infinitely dense and specify a one-to-one mapping between the network and the square.
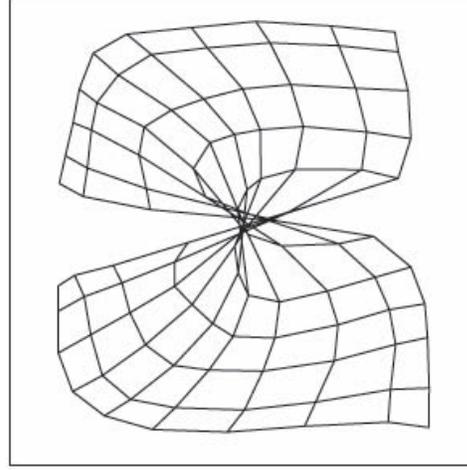
Abb. 5.6: An example of an incompletely ordered state of the network, evolved as a consequence of the range $\sigma(t)$ of $h_{\mathbf{rs}}$ to be too short initially (see Eq. (68)). In this case a topological defect develops and the connections between neighboring lattice points cross. In the continuum limit a one-to-one mapping cannot be obtained.

We consider an ensemble of maps that, after t learning steps, are all in the vicinity of the same asymptotic state and whose distribution is given by a distribution function $S(\mathbf{w}, t)$. In the limit $t \to \infty$, $S(\mathbf{w}, t)$ converges towards a stationary distribution $S(\mathbf{w})$ with a mean value $\bar{\mathbf{w}}$. In Chapter 14 we will show that the variance of $S(\mathbf{w})$ under the given conditions will be of the order of ϵ. Therefore, for an ϵ that is sufficiently slowly approaching zero, all members of the ensemble will result in the same map characterized by its value $\bar{\mathbf{w}}$.

We want to calculate $\bar{\mathbf{w}}$ in the limit $\epsilon \to 0$. In the stationary state, the condition $S(\mathbf{w}) = \int Q(\mathbf{w}, \mathbf{w}')S(\mathbf{w}') \, d\mathbf{w}'$ holds, and, therefore, it also holds that

$$\bar{\mathbf{w}} = \int \mathbf{w}S(\mathbf{w}) \, d\mathbf{w} = \int \int \mathbf{w}Q(\mathbf{w}, \mathbf{w}')S(\mathbf{w}') \, d\mathbf{w}d\mathbf{w}'. \qquad (5.6)$$

In the limit $\epsilon \to 0$ it follows $S(\mathbf{w}) \to \delta(\mathbf{w} - \bar{\mathbf{w}})$ and, therefore,

$$
\begin{aligned}
\bar{\mathbf{w}} &= \int \mathbf{w} Q(\mathbf{w}, \bar{\mathbf{w}}) \, d\mathbf{w} \\
&= \int \mathbf{T}(\bar{\mathbf{w}}, \mathbf{v}, \epsilon) P(\mathbf{v}) \, d\mathbf{v}.
\end{aligned}
\tag{5.7}
$$

Applying Eq. (5.5) we obtain

$$
0 = \epsilon \int h_{\mathbf{rs}}(\mathbf{v} - \bar{\mathbf{w}}_{\mathbf{r}}) P(\mathbf{v}) \, d\mathbf{v} \quad \text{for all } \mathbf{r} \in A.
\tag{5.8}
$$

We formulate the restriction of maximally ordered maps by two approximating assumptions:

1. We assume that for sufficiently large systems $\bar{\mathbf{w}}_{\mathbf{r}}$ is a function that varies slowly from lattice point to lattice point so that its replacement by a function $\bar{\mathbf{w}}(\mathbf{r})$ on a continuum of $\mathbf{r}$-values is justified.

2. We assume that $\bar{\mathbf{w}}(\mathbf{r})$ is one-to-one.

We demand also that $h_{\mathbf{rs}}$ at $\mathbf{r} = \mathbf{s}$ has a steep maximum and satisfies

$$
\begin{aligned}
\int h_{\mathbf{rs}}(\mathbf{r} - \mathbf{s}) \, d\mathbf{r} &= 0, \\
\int h(\mathbf{r} - \mathbf{s})(r_i - s_i)(r_j - s_j) \, d\mathbf{r} &= \delta_{ij}\sigma^2, \quad i, j = 1, \ldots, d
\end{aligned}
\tag{5.9}
$$

where d is the dimension of V and r_j, s_j describe the d Cartesian components of $\mathbf{r}$, $\mathbf{s}$. The constant σ is the range of $h_{\mathbf{rs}}$ which coincides with σ in (68) in case of a Gaussian $h_{\mathbf{rs}}$.

From the above we will derive a differential equation for $\bar{\mathbf{w}}$. Due to the continuum approximation (i), the quantity $\min_{\mathbf{r} \in A} \|\mathbf{w}_{\mathbf{r}} - \mathbf{v}\|$ in Eq. (5.7) vanishes because now for each $\mathbf{v}$ there exists exactly one $\mathbf{r}$ for which $\mathbf{w}_{\mathbf{r}} = \mathbf{v}$ holds. Therefore, we can replace $\mathbf{v}$ in Eq. 5.8) by $\bar{\mathbf{w}}(\mathbf{s})$. Here $\mathbf{s} := \phi_{\bar{\mathbf{w}}}(\mathbf{v})$ is the image of $\mathbf{v}$ under the map that belongs to $\bar{\mathbf{w}}$. This provides the condition

$$
\int h_{\mathbf{rs}}\left(\bar{\mathbf{w}}(\mathbf{s}) - \bar{\mathbf{w}}(\mathbf{r})\right) P(\bar{\mathbf{w}}(\mathbf{s})) J(\mathbf{s}) \, d\mathbf{s} = 0.
\tag{5.10}
$$

Here

$$
J(\mathbf{s}) := \left| \frac{d\mathbf{v}}{d\mathbf{s}} \right|
\tag{5.11}
$$

is the absolute value of the Jacobian of the map $\phi_{\bar{\mathbf{w}}}$. With $\mathbf{q} := \mathbf{s} - \mathbf{r}$ as a new integration variable and $\bar{P}(\mathbf{r}) := P(\bar{\mathbf{w}}(\mathbf{r}))$ the expansion of Eq. (5.10) in powers of $\mathbf{q}$ yields (with implicit summation over repeated indices; *e.g.*, $q_i \partial_i$ is to be summed over all values of i)

$$
\begin{aligned}
0 &= \int h_{\mathbf{q}0}(q_i \partial_i \bar{\mathbf{w}} + \frac{1}{2} q_i q_j \partial_i \partial_j \bar{\mathbf{w}} + \ldots) \cdot \\
&\qquad \cdot (\bar{P} + q_k \partial_k \bar{P} + \ldots) \cdot (J + q_l \partial_l J + \ldots) \, d\mathbf{q} \\
&= \int h_{\mathbf{q}0} q_i q_j \, d\mathbf{q} \cdot \left((\partial_i \bar{\mathbf{w}}) \partial_j (\bar{P}J) + \frac{1}{2} \bar{P}J \cdot \partial_i \partial_j \bar{\mathbf{w}} \right)(\mathbf{r}) + O(\sigma^4) \\
&= \sigma^2 \cdot \left[(\partial_i \bar{\mathbf{w}})(\partial_i (\bar{P}J) + \frac{1}{2} \bar{P}J \cdot \partial_i^2 \bar{\mathbf{w}}) \right](\mathbf{r}) + O(\sigma^4),
\end{aligned}
\tag{5.12}
$$

where we made use of (81). In order for the expansion (5.12) to hold it is necessary and sufficient for small σ that condition

$$
\sum_i \partial_i \bar{\mathbf{w}} \left(\frac{\partial_i \bar{P}}{\bar{P}} + \frac{\partial_i J}{J} \right) = -\frac{1}{2} \sum_i \partial_i^2 \bar{\mathbf{w}}
\tag{5.13}
$$

or, with the Jacobi matrix $J_{ij} = \partial_j \bar{w}_i(\mathbf{r})$ and $\Delta = \sum_i \partial_i^2$, condition

$$
\mathbf{J} \cdot \nabla \ln(\bar{P} \cdot J) = -\frac{1}{2} \Delta \bar{\mathbf{w}}
\tag{5.14}
$$

is satisfied. For the one-dimensional case we obtain $\mathbf{J} = J = d\bar{w}/dr$ and $\Delta \bar{\mathbf{w}} = d^2\bar{w}/dr^2$ with $\bar{w}$ and r as scalars. In this case the differential equation (5.14) can be solved. For this purpose we rewrite (5.14) and obtain

$$
\frac{d\bar{w}}{dr} \left(\frac{1}{\bar{P}} \frac{d\bar{P}}{dr} + \left(\frac{d\bar{w}}{dr} \right)^{-1} \frac{d^2\bar{w}}{dr^2} \right) = -\frac{1}{2} \frac{d^2\bar{w}}{dr^2}
\tag{5.15}
$$

from which we can conclude

$$
\frac{d}{dr} \ln \bar{P} = -\frac{3}{2} \frac{d}{dr} \ln \left(\frac{d\bar{w}}{dr} \right).
\tag{5.16}
$$

This result allows us to determine the local enlargement factor of the map in terms of the generating probability distribution $P(\mathbf{v})$.

Since $\phi_{\bar{\mathbf{w}}}(\bar{\mathbf{w}}(\mathbf{r})) = \mathbf{r}$ holds, the local enlargement factor M of $\phi_{\bar{\mathbf{w}}}$ can be defined by $M = 1/J$ (compare Eq. (5.11)). For the one-dimensional case $M =$

$(d\bar{w}/dr)^{-1}$ and we obtain as a relation between input stimulus distribution and cortical representation

$$M(v) = J^{-1} = \frac{dr}{d\bar{w}} \propto P(v)^{2/3}. \tag{5.17}$$

The local enlargement factor $M(v)$ depends on the probability density $P(v)$ according to a power law. It can be shown that the exponent $2/3$ that we found in the continuum approximation undergoes a correction for a discrete one-dimensional system and is then given by $\frac{2}{3} - [3(1 + n^2)(1 + [n+1]^2)]^{-1}$, where n is the number of neighbors that are taken into account on each side of the excitation center, (*i.e.*, $h_{\mathbf{rs}} = 1$ for $\|\mathbf{r} - \mathbf{s}\| \leq n$ and zero elsewhere) (Ritter 1989). The continuum corresponds to the limit of infinite density of neighbors. Then $n = \infty$ for each finite σ and we obtain the previous result of $2/3$.

5.5 "Cortical Representation" in the Model of the Bat's Auditory Cortex

We now apply the mathematical derivation of Section 5.4 to the particular input stimulus distribution that we assumed for our model of the bat's auditory cortex and compare the result with a simulation.

The input stimulus distribution that we assume can be written in the range $v_1 \leq v \leq v_2$ as

$$P(v) = \frac{P_0}{v_2 - v_1} + (1 - P_0)\frac{1}{\sqrt{2\pi}\sigma_r} \exp\left(-\frac{(v - v_e)^2}{2\sigma_r^2}\right) \tag{5.18}$$

with the parameters σ_r=0.5 kHz, v_e=61.0 kHz, v_1=20 kHz, v_2=100 kHz and P_0=1/4. The width of the distribution of the Doppler-shifted echoes is given by σ_r, and P_0 is the probability for the occurrence of an input stimulus from the white background noise. v_1 and v_2 are the limits of the ultrasound spectrum that we assume the bat can hear.

The integral $I = \int_{v_1}^{v_2} P(v)dv$ is not exactly unity because of the finite integration limits. Since, due to the small σ_r of 0.5 kHz, nearly all the Doppler-shifted echo signals lie within the interval $[20, 100]$ and the deviation of I from unity is negligible. With the choice $P_0 = 1/4$, the Doppler-shifted signals occur three times as often as signals due to the background noise (see

also Fig. 5.2). From Eqs. (5.17) and (5.18) we find

$$\frac{dr}{d\bar{w}} = C \cdot \left(\frac{P_0}{v_2 - v_1} + (1 - P_0)\frac{1}{\sqrt{2\pi}\sigma_r} \exp\left(-\frac{(v - v_e)^2}{2\sigma_r^2}\right) \right)^{2/3} \qquad (5.19)$$

where C is a proportionality constant. In integral form one has

$$r(\bar{w}) - r_1 = C \cdot \int_{\bar{w}_1}^{\bar{w}} \left(\frac{P_0}{v_2 - v_1} + \frac{1 - P_0}{\sqrt{2\pi}\sigma_r} \right.$$
$$\left. \times \exp\left(-\frac{(v - v_e)^2}{2\sigma_r^2}\right) \right)^{2/3} dv. \qquad (5.20)$$

We will solve this integral numerically and then compare the resulting $\bar{w}(r)$ with the corresponding values from a simulation.

Since these considerations apply only to the case where the dimensionality of the net and the dimensionality of the space of input stimuli is identical, we stretch the "auditory cortex" and, instead of a 5×25 net as in Figs. 5.3 and 5.4, assume a one-dimensional chain with 50 elements for the present simulation. Starting from a linear, second-order differential equation, we need two boundary conditions, $e.g.$, $\bar{w}_1(r_1)$ and $\bar{w}_2(r_2)$, from our simulation data to be able to adjust the function $r(\bar{w})$ of Eq. (5.20) uniquely. Since boundary effects at the beginning and the end of the chain were not taken into account in our analytic calculation, the end points can in some cases deviate slightly from our calculated curve. To adjust the curve to the simulation data, we take values for w_1 and w_2 that do not lie too close to the end points; in this case we have chosen $\bar{w}$ at the third and forty-eighth link of the chain, $i.e.$, at $r_1 = 3$ and $r_2 = 48$. The solid curve in Fig. 5.6 depicts the function $\bar{w}(r)$ calculated numerically from Eq.(5.20) and adjusted to the simulation data. The dots show the values $\bar{w}_r$ that were obtained by simulating the Markov process (75). The representation corresponds to the one in Fig. 5.4. The time dependence of the excitation zone σ and of the adaptation step width ϵ for the simulation were chosen as follows: $\sigma(t) = \sigma_i[1 + \exp(-(5t/t_{max})^2)]$ with $\sigma_i = 10$, $\epsilon(t) = \epsilon_i \exp(-(5t/t_{max})^2)$ with $\epsilon_i = 1$. For the maximal number of learning steps $t_{max} = 20000$ was chosen.
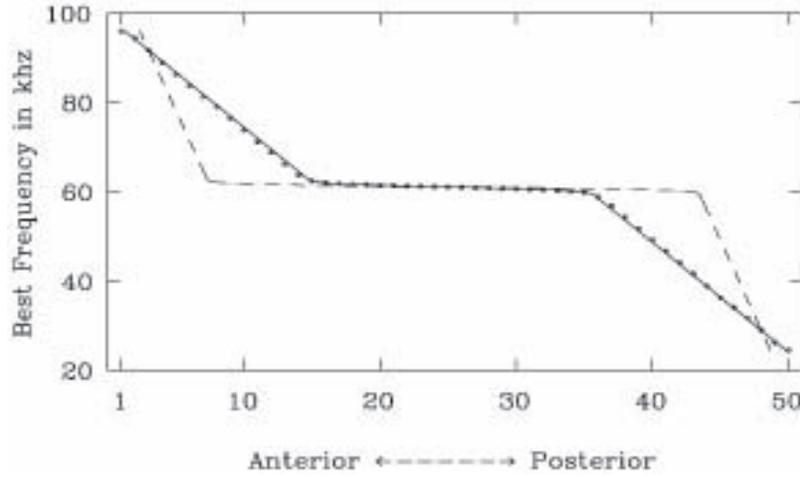
Abb. 5.7: A bat's sensitivity to accoustic and sonar signals (cf. Fig. 5.4). The solid curve represents the function $\bar{w}(r)$ calculated from Eq. (92). The dots show the values obtained from simulating the Markov process (75). For comparison we show the result for $M(v) \propto P(v)$ with a dashed line. This result strongly deviates from the simulation data.

Clearly, the function $\bar{w}(r)$ resulting from Eq. (5.20) is in close agreement with the simulation results, and even the deviations at the end points are small. One may have expected intuitively that for the magnification holds $M(v) \propto P(v)$, *i.e.*, a magnification proportional to the stimulus density. The corresponding result is presented in Fig. 5.6 as well to demonstrate that this expectation is, in fact, incorrect.

For the present input stimulus distribution, it is possible to estimate the size of the region relevant for the analysis of the Doppler-shifted signal, *i.e.*, the extension of the 61 kHz plateau in Fig. 5.6. In Eq. 5.20) we integrate over $P(v)^{2/3}$ and, therefore, the function $r(\bar{w})$ increases sharply for large values of $P(v)$. Hence, the plateau starts where the Gaussian distribution of the Doppler-shifted echoes increases strongly relative to the background. This is approximately the case for $v = v_e - 2\sigma_r$. Accordingly, the plateau ends where the Gaussian peak recedes back into the homogeneous background, *i.e.*, at $v = v_e + 2\sigma_r$. Therefore, the relation

$$\Delta r_{plateau} = C \cdot \int_{v_e-2\sigma_r}^{v_e+2\sigma_r} \left(\frac{P_0}{v_2 - v_1} + (1 - P_0) \frac{1}{\sqrt{2\pi}\sigma_r} \right)$$

$$\times \exp\left(-\frac{(v-v_e)^2}{2\sigma_r^2}\right)\right)^{2/3} dv \tag{5.21}$$

for the size of the plateau holds. Within these integration limits the background portion in the integrand is negligible compared to the values of the Gaussian. Furthermore, we can extend the integration of the integrand that results without the background towards infinity without significant error. The integral can then be evaluated, yielding the approximation

$$\Delta r_{plateau} \approx C \cdot (1-P_0)^{2/3} \int_{-\infty}^{\infty} \frac{1}{(\sqrt{2\pi}\sigma_r)^{2/3}} \exp\left(-\frac{2}{3}\frac{v^2}{2\sigma_r^2}\right) dv$$

$$\approx C \cdot \sqrt{\frac{3}{2}} \left(\sqrt{2\pi}\sigma_r(1-P_0)^2\right)^{1/3}. \tag{5.22}$$

In order to determine the part of the plateau relative to the overall "auditory cortex," we also need an estimate of the integral in Eq. (5.20), where we have to integrate over the full band width of input frequencies. To obtain this we split the integration range from $v_1=20\,\text{kHz}$ to $v_2=100\,\text{kHz}$ into three regions as follows

$$\Delta r_{total} \propto \int_{v_1}^{v_e-2\sigma_r} (P(v))^{2/3} dv + \int_{v_e-2\sigma_r}^{v_e+2\sigma_r} (P(v))^{2/3} dv$$

$$+ \int_{v_e-2\sigma_r}^{v_2} (P(v))^{2/3} dv. \tag{5.23}$$

We have already estimated the second integral in the sum by Eq. (5.22). Within the integration limits of the other two integrals the contribution of the Gaussian distribution is so small that it can be neglected relative to the background. In addition, $\sigma_r \ll (v_2 - v_1)$, enabling us to write

$$\Delta r_{total} \approx \Delta r_{plateau} + C \cdot (v_2 - v_1) \left(\frac{P_0}{v_2 - v_1}\right)^{2/3}$$

$$\approx \Delta r_{plateau} + C \cdot P_0^{2/3}(v_2 - v_1)^{1/3}. \tag{5.24}$$

If we insert the parameters of our above model of the input stimulus distribution of the bat into the two estimates (5.22) and (5.24), we obtain for the size of the 61 kHz region, relative to the size of the total "cortex," the value

$$\frac{\Delta r_{plateau}}{\Delta r_{total}} \approx 39\%.$$

This implies that for our case of a 50-unit chain, the plateau should consist of 19 to 20 neurons. This value agrees very well with the simulation results presented in Fig. 5.6.

By now we have extensively described the basics of Kohonen's model—the self-organization of a topology-conserving map between an input stimulus space and a network of neural units. We have compared the simulation results of Kohonen's model to experimental data as well as to a mathematical description valid for certain limiting cases. The simulation data have agreed at least qualitatively with the experimental findings. More than a qualitative agreement should not have been expected, considering the many simplifications of Kohonen's model. In contrast to that, the mathematical result for the representation of the input signals relative to their probability corresponds, even quantitatively, very well to the results obtained from simulations.

In Chapter 6 we will become acquainted with a completely different application of Kohonen's model. Instead of a mappingonto a continuum, we will generate a mapping that projects a linear chain onto a discrete set of points. Such a mapping can be interpreted as a choice of a connection path between the points. The feature of the algorithm to preserve topology as much as possible manifests itself in a tendency to minimize the path-length. In this way, very good approximate solutions for the well-known travelling salesman problem can be achieved.